ACS OMEGA

Open Access

http://pubs.acs.org/journal/acsodf

Article

Toward Non-Invasive Neurological Biomarker Monitoring: Dopamine Sensing in Tears with Laser-Induced Graphene Electrochemical Sensors

Lucas Minghini Gonçalves, Bruno Vasconcellos Lopes, Bruno da Silveira Noremberg, Raphael Dorneles Caldeira Balboni, Guilherme Kurz Maron, Anderson Thesing, Daiane Dias, Irene Teresinha Santos Garcia, Sabir Khan, and Neftali Lenin Villarreal Carreno*

Cite This: *ACS Omega* 2026, 11, 36141−36150

Read Online

ACCESS | Metrics & More | Article Recommendations | Supporting Information

ABSTRACT: Dopamine plays a crucial role in motor control, cognition, and emotional regulation, and its abnormal levels are associated with disorders such as Parkinson's disease and schizophrenia, highlighting the need for sensitive, selective, and noninvasive detection methods. This study reports the development of a high-performance, nonenzymatic electrochemical sensor based on laser-induced graphene, functionalized with nickel nitrate and urea, for the detection of dopamine. Cyclic voltammetry and differential pulse voltammetry were employed to assess the sensor's selectivity and overall performance. In-depth characterization by scanning electron microscopy and Raman spectroscopy confirmed the successful formation of a porous and electroactive graphene structure, uniformly functionalized with nickel ions and nitrogen-containing groups. These modifications enhanced electron transfer rates and increased the number of active sites for dopamine oxidation. Electrochemical measurements demonstrated excellent performance, with a linear detection range of 0.25−16.44 μmol·L^{-1}, a limit of detection of 17.86 nmol·L^{-1}, and a limit of quantification of 54.14 nmol·L^{-1}, with R^2 = 0.98 in phosphate-buffered solution. In synthetic tear fluid, the sensor maintained a reliable response across four different concentrations ranging from 3.23 to 9.32 μmol·L^{-1}. Furthermore, the sensor exhibited excellent analytical performance in real matrices, achieving recovery rates close to 100% in real sample analyses.

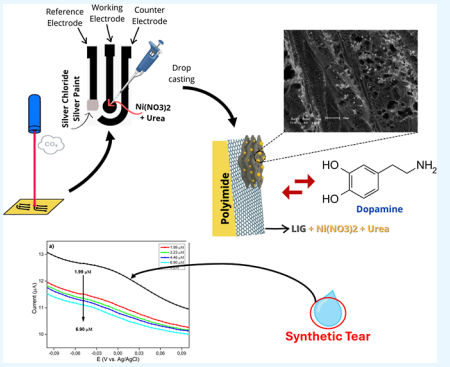

1. INTRODUCTION

Dopamine (DA) is a catecholaminergic neurotransmitter essential to the central nervous system, playing a critical role in modulating cognitive, motor, and reward processes, acting as a mediator of the sensation of well-being.[1] Epidemiological studies have shown that alterations in DA levels are associated with neurodegenerative and psychiatric disorders, including Parkinson's disease, schizophrenia, Alzheimer's disease, and depression.[2,3] These conditions are directly related to dysfunctions in dopaminergic systems.[4]

For healthy individuals, plasma DA concentrations range between 0 and 30 pg·mL^{-1} (195.8 pmol·L^{-1}),[5] while in tear fluid measured via the Schirmer technique, reported levels range from 152 to 519.1 pg·mL^{-1} (3.38 μmol·L^{-1}).[6,7] Currently, DA monitoring is predominantly based on invasive methods such as urine analysis, blood sampling, or brain implants. While effective, these approaches present limitations regarding practicality, patient risk, and discomfort.[8,9]

As a promising and yet noncommercialized alternative, electrochemical sensors have emerged as a promising alternative for the detection of DA in biological fluids due to their high sensitivity, selectivity, and possibility of miniaturization.[10,11] These devices convert chemical interactions between the analyte and the electrode into measurable electrical signals, offering advantages such as low cost,[12,13] portability,[14] and the ability for *in situ* analysis. The chemical composition of these sensors plays a fundamental role in their performance and applicability, often relying on conductive materials, semiconductors, or nanocomposites to enhance sensitivity and selectivity.[15] The electrochemical performance of sensors is intrinsically associated with the architecture of the transducer material.[16,17]

In this context, carbon-based materials—especially graphene—have emerged as ideal platforms due to their high conductivity, large surface area, and chemical stability.[18] Laser-induced graphene (LIG) obtained via laser carbonization of polymeric substrates represents a significant advancement in

Received: March 25, 2026
Revised: June 1, 2026
Accepted: June 3, 2026
Published: June 9, 2026

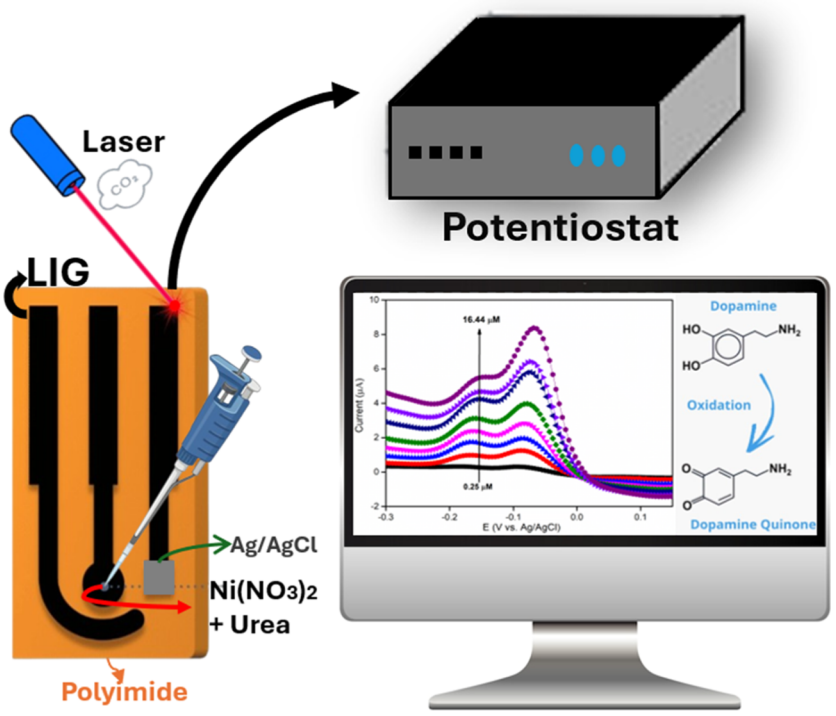

Figure 1. Schematic representation of the LIG fabrication process, leading to the results with dimensions of 10 × 20 mm.

this field. LIG exhibits a three-dimensional porous structure, tunable electrocatalytic properties, and compatibility with scalable manufacturing processes.[19] Due to its ease of fabrication and low cost, LIG has been widely explored for application in wearable devices, environmental monitoring, and health.[20−22] Urea was employed within the LIG framework to enhance pore enlargement, thereby facilitating the deposition of nickel particles.[23,24] In parallel, nickel-based compounds have attracted interest in sensor development due to their redox activity, low cost, and electrocatalytic efficiency.[25] Moreover, functionalizing the LIG surface with nickel can enhance sensitivity and selectivity toward specific molecules such as DA through an electronic coordination mechanism.[26]

In this study, we report on the development of a low-cost, nonenzymatic electrochemical sensor based on LIG functionalized with nickel nitrate and urea for the detection of DA under standard laboratory conditions and synthetic tear fluid. Cyclic voltammetry (CV) and differential pulse voltammetry (DPV) were employed to evaluate the sensor's electroanalytical performance, with a focus on clinical diagnostics and noninvasive monitoring applications.

2. EXPERIMENTAL SECTION

2.1. Materials

Sodium dihydrogen phosphate and disodium hydrogen phosphate were supplied by Synth (São Paulo, Brazil). Nickel(II) nitrate hexahydrate, urea, dopamine hydrochloride, L-lactate, β-D-glucose, L-ascorbate, and bovine serum albumin were supplied by Sigma-Aldrich (São Paulo, Brazil). All chemicals used in the experiments were analytical grade. Ultrapure water (25 °C), obtained from a Milli Q Direct-0.3 purifier (Millipore), was used for both the preparation of the solutions and the synthesis of the materials.

2.2. Electrode Fabrication and Functionalization

Three-electrode platforms were developed for sensor fabrication, comprising a working, counter, and reference electrodes. Electrode layouts were designed in Inkscape vector graphics software. The electrodes were fabricated via a two-step carbonization process using direct laser writing (DLW) on polyimide (Kapton) film. A CO_2 laser (10.2 μm) engraving machine (Visutec Router VS3020P) was employed, operating at a scan speed of 100 mm·s^{-1} and a power output of 3.2 W. In the first step, the laser was used to engrave the Kapton film, creating a complete three-electrode design. For the preparation of the structure-modifying solution for LIG, 0.1 mol·L^{-1} nickel nitrate and 0.3 mol·L^{-1} urea were dissolved in ultrapure water. The working electrode was then modified via drop-casting with 20 μL of an aqueous solution of 0.1 mol·L^{-1} nickel nitrate and 0.3 mol·L^{-1} urea. After allowing it to dry for 4 h, a second DLW was applied to further process the modified layer. Different functionalization was tested, including the combinations of LIG/urea, LIG/$Ni(NO_3)_2$, and LIG/$Ni(NO_3)_2$ + Urea. To determine the optimal urea concentration, sensors were also tested with concentrations ranging from 0.1 to 0.4 mol·L^{-1}. A layer of commercial Ag/AgCl conductive ink (ALS da BAS Inc., Tokyo, Japan) was applied to the pseudoreference electrode. Conductive silver ink was applied to all three electrodes to improve electrical contact. Finally, a hot-glue barrier was added around the electrode area to create a containment well for the electrolyte solution to be deposited during electrochemical measurements. Figure 1 illustrates the methodology used for electrode fabrication.

2.3. Apparatus

Raman spectroscopy was performed using a WITec alpha300 confocal Raman microscope equipped with a 50× objective and a 532 nm excitation laser. All samples were analyzed under identical experimental conditions, with an integration time of 1 s and 60 accumulated scans, and with laser power maintained constant across measurements. For each electrode, spectra were collected from three different regions and averaged to ensure a representative sampling. The acquired spectra underwent sequential processing, including baseline correction through polynomial fitting, normalization, and Gaussian smoothing with a standard deviation of 10. Spectral analysis focused on integrated peak areas rather than relative intensities to ensure an accurate quantitative comparison. Control measurements conducted on replicate samples prepared under identical conditions confirmed the reproducibility of the spectra with no observable significant peak shifts between measurements. This rigorous analytical approach ensured the reliable characterization of carbonaceous

https://doi.org/10.1021/acsomega.6c03287
ACS Omega 2026, 11, 36141−36150

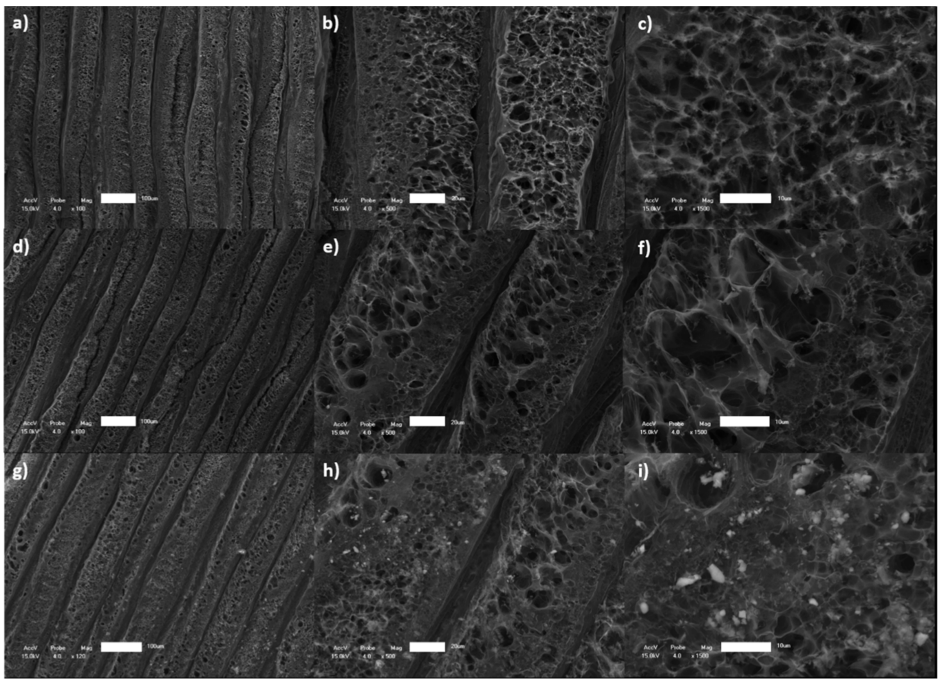

Figure 2. Comparative SEM micrographs of (a–c) LIG, (d–f) LIG/Urea, and (g–i) LIG/$Ni(NO_3)_2$ + Urea composites at different magnification levels.

materials while minimizing measurement variability. The consistent experimental parameters across all samples enabled a direct comparison of spectral features between different material compositions. Scanning electron microscopy (SEM) was performed using a Shimadzu SSX-550, at magnifications of 100×, 500×, and 1500×, to investigate LIG morphology. All electrochemical tests were conducted on a Metrohm Autolab PGSTAT302N potentiostat/galvanostat.

2.4. Preparation of Solutions and Real Samples

For the blank sensor samples, a 0.1 mol·L^{-1} PBS solution was used, prepared using $NaH_2PO_4{\cdot}H_2O$ and Na_2HPO_4 in distilled water, followed by 10 min of sonication. The analytical solution consisted of 1 mmol·L^{-1} DA, prepared by dissolving dopamine hydrochloride in 0.1 mol·L^{-1} PBS and sonicating it for 10 min. The synthetic tear solution was prepared following the protocol by Reid (2015)[27] and included 150 mmol·L^{-1} PBS, 3 mmol·L^{-1} L-lactate, 0.05 mmol·L^{-1} β-D-glucose, 0.18 mmol·L^{-1} L-ascorbate, 5.4 mmol·L^{-1} urea, and 0.2 mg·mL^{-1} BSA. For performance evaluation, triplicate measurements were performed using CV and DPV. An interference study was conducted, where each synthetic tear component was individually mixed with the 1 mmol·L^{-1} DA solution to analyze the behavior of the LIG/$Ni(NO_3)_2$ + Urea sensor, as shown in Figure S4.

2.5. Electrochemical Measurements

Electrochemical experiments were used to evaluate the sensor's working range, DA detection capability, and the corresponding current responses. CV measurements were conducted in the potential window from −0.5 to 0.5 V at a scan rate of 0.05 V·s^{-1}. DPV tests were performed from −0.35 to 0.35 V, with a step potential of 0.005 V, and a scan rate of 0.05 V·s^{-1}. Before each test, the sensor was activated by applying five CV cycles in 400 μL of 0.1 mol·L^{-1} PBS. A baseline analysis was then recorded and used as a reference to calculate current differences in DA presence. The PBS was then replaced with 400 μL of 100 μmol·L^{-1} dopamine solution. Analytical curves were constructed based on oxidation peak currents from DPV triplicates. Mean and standard deviation values were calculated. DA concentrations ranged from 0.25 to 16.44 μmol·L^{-1} in PBS, and from 1.99 to 6.90 μmol·L^{-1} in synthetic tears.

3. RESULTS AND DISCUSSION

3.1. Physical-Chemical Characterization of the Electrodes

During laser irradiation of the polyimide substrate surface, different structural configurations of LIG can be obtained. These configurations vary according to the laser beam's incidence parameters and the irradiation pattern (linear or dot).[28] The LIG exhibits a highly interconnected porous structure composed of three-dimensional graphene nanosheets, which are considered ideal for electrochemical sensor electrodes.[19,29] The SEM images were used to analyze the matrix structure of LIG, LIG/Urea, and LIG/$Ni(NO_3)_2$ + Urea. The analysis revealed that the LIG's structural behavior was modified, with pore growth and particle deposition within the porous structures. Figure 2a–c) shows the SEM analysis of the LIG samples at different magnifications. Functionalization with urea led to significant morphological changes, as evidenced by an increase in pore size at higher magnification (Figure 2d–f). The thermal decomposition of urea during laser irradiation released gases that generated internal pressure and promoted structural exfoliation, resulting in larger pores.[30,31] SEM analysis of the LIG/$Ni(NO_3)_2$ + Urea sample (Figure 2g–i)), conducted at different magnification levels, revealed a uniform distribution of microparticles within the carbon matrix. These nickel-derived particles embedded in the LIG matrix may act as electrical current amplifiers in the electrochemical sensor, thereby enhancing electrocatalytic activity.[32,33]

To verify the presence of nitrogen functionalization, CHN elemental analysis was conducted to quantify nitrogen-containing groups in four different material systems: pristine LIG, LIG/Urea, LIG/$Ni(NO_3)_2$, and LIG/$Ni(NO_3)_2$ + Urea. As shown in Table S1, the LIG/$Ni(NO_3)_2$ + urea composite exhibited a 13.08% increase in nitrogen content compared to the corresponding formulation without urea. This result confirms the successful incorporation of nitrogen into the

https://doi.org/10.1021/acsomega.6c03287
ACS Omega 2026, 11, 36141−36150

carbon-based matrix of the LIG. As reported before, nitrogen-rich functional groups may enhance electrical signal amplification, highlighting their importance in improving the electrochemical performance of the sensor.[34]

In the Raman spectra of LIG, the D, G, and 2D bands are key indicators of the material's structure and quality. The Raman spectroscopy of the samples is shown in Figure 3. The

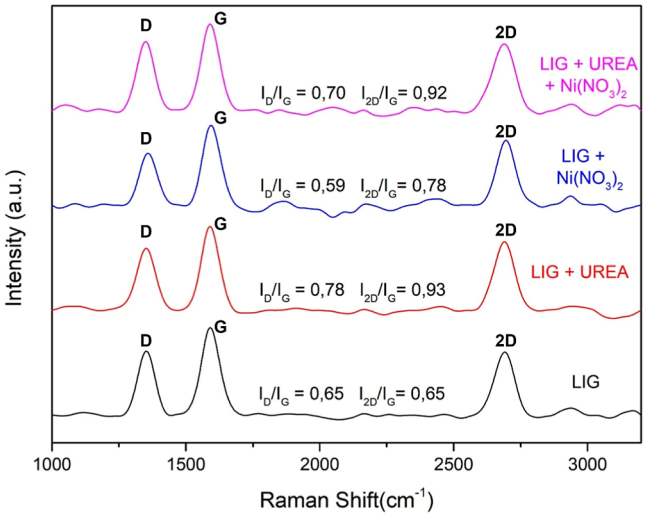

Figure 3. Raman spectra of LIG, LIG/Urea, LIG/$Ni(NO_3)_2$, and LIG/$Ni(NO_3)_2$ + Urea electrodes.

G band is associated with the in-plane stretching of sp^2 carbon atoms, and it provides information about the ordering within the graphitic structure. The D band reflects structural disorder and defects in the carbon lattice, such as vacancies, sp^3 hybridization, or edge effects, and becomes active in the presence of imperfections, i.e., higher intensity in this band indicates a greater level of disorder. The 2D band is a second-order overtone of the D band and is related to the stacking order and number of graphene layers.[31,35] The analysis of the relative intensities of these bands, specifically the I_D/I_G and I_{2D}/I_G ratios, is essential to evaluate the degree of graphitization and defect density in LIG. As illustrated in Figure 3, nitrogen incorporation via urea doping increases the I_D/I_G ratio, reflecting greater structural disorder and defect density in the graphene lattice. This behavior is typical of oxidation processes or heteroatom introduction, as supported by the CHN elemental analysis. The increase in the I_{2D}/I_G ratio observed after doping suggests a decrease in the number of graphene layers. Therefore, the simultaneous increase in the I_D/I_G ratio suggests that nitrogen doping reduces the number of graphene layers while increasing defect density.[36,37]

To reinforce the results and the process of nitrogen incorporation, FTIR analysis (Figure S1) was performed to understand, which functional groups are present on the sensor's surface. The FTIR analysis of the LIG/$Ni(NO_3)_2$ + urea sensor confirms the successful functionalization of the LIG matrix. A broad band at 3594 cm^{-1} is attributed to the O−H and N−H stretching vibrations,[38] originating from both residual moisture and the urea precursor. The characteristic Amide I band, dominated by the C═O stretching vibration, is observed at 1654 cm^{-1}, while the Amide II band, primarily resulting from N−H in-plane bending, appears at 1541 cm^{-1}.[39] The presence of both bands provides strong evidence of effective urea integration. Furthermore, the peak at 1504 cm^{-1} corresponds to the C═C stretching of the LIG aromatic skeleton, while the signal at 1702 cm^{-1} suggests C═O stretching from residual oxidation during the laser induction process.[40] Regarding the nitrogenous and metallic species, the peaks at 1459 cm^{-1} (C−N stretching), 1397 cm^{-1} (asymmetric NO_3^- stretching), and 670 cm^{-1} (Ni−O/Ni−OH lattice vibrations) confirm the successful incorporation of nickel nitrate and urea into the sensor's active surface.[41−43]

3.2. Electrochemical Results

To investigate the electrochemical detection capability of the LIG/$Ni(NO_3)_2$ + Urea electrode, CV measurements were carried out in the absence and presence of DA, and the results are shown in Figure 4a. As reported in the literature, sensors based on carbonaceous materials exhibit high reactivity toward DA oxidation.[32,44] The superior electrocatalytic performance of the LIG electrode modified with nickel nitrate and urea is attributed to the synergistic effect between the nickel nanoparticles and nitrogen doping within the graphene matrix. During the laser writing process, the thermal decomposition of urea not only promotes the formation of a highly porous graphene structure, with an increased effective surface area, but also facilitates the incorporation of nitrogen active sites, which modulate the local electronic density and favor the adsorption of dopamine molecules.[32,45]

The oxidation mechanism of dopamine involves the transfer of two electrons and two protons to form dopamine quinone (DAQ), a process catalyzed by the presence of nickel species (such as NiO or $Ni(OH)_2$/NiOOH), which act as redox mediators and signal amplifiers.[46,47] Simulations based on density functional theory in analogous systems indicate that the interaction between the nickel metal centers and the nitrogen-functionalized groups reduces the activation energy for interfacial charge transfer, resulting in more defined oxidation peaks and significantly higher peak currents compared to unmodified LIG.[32,48] This hybrid architecture not only enhances the electrical conductivity of the sensor but also stabilizes the catalytic sites, ensuring high sensitivity and selectivity even in complex matrixes, such as synthetic tear fluid. A well-defined oxidation peak was observed at 0.04 V, demonstrating that the electrode exhibits a sensing capability for DA oxidation.

At this potential, the catechol group in the dopamine molecule undergoes oxidation, forming dopamine-o-quinone through the loss of two electrons and two protons. This redox transformation involves the formation of covalent bonds between the aromatic ring and adjacent oxygen atoms, as illustrated in the inset of Figure 4a. In the subsequent reduction step, observed near −0.1 V, the quinone structure is reduced back to dopamine, completing the reversible redox cycle.[49]

To investigate and determine the optimal urea concentration for DA detection, CV measurements were performed using LIG/$Ni(NO_3)_2$ electrodes and urea concentrations ranging from 0.1 to 0.4 mol·L^{-1} (Figure 4b). The tests were conducted in a 100 μmol·L^{-1} DA solution, using PBS as the supporting electrolyte. The inset displays the values of the current response for each sensor. The highest current response was observed for the sensor functionalized with 0.3 mol·L^{-1} urea. These results can be attributed to the synergistic effect between the nickel-based particles and the nitrogen doping introduced by urea functionalization. As demonstrated in the SEM, urea enhances the porosity of the LIG structure, while

https://doi.org/10.1021/acsomega.6c03287
ACS Omega 2026, 11, 36141−36150

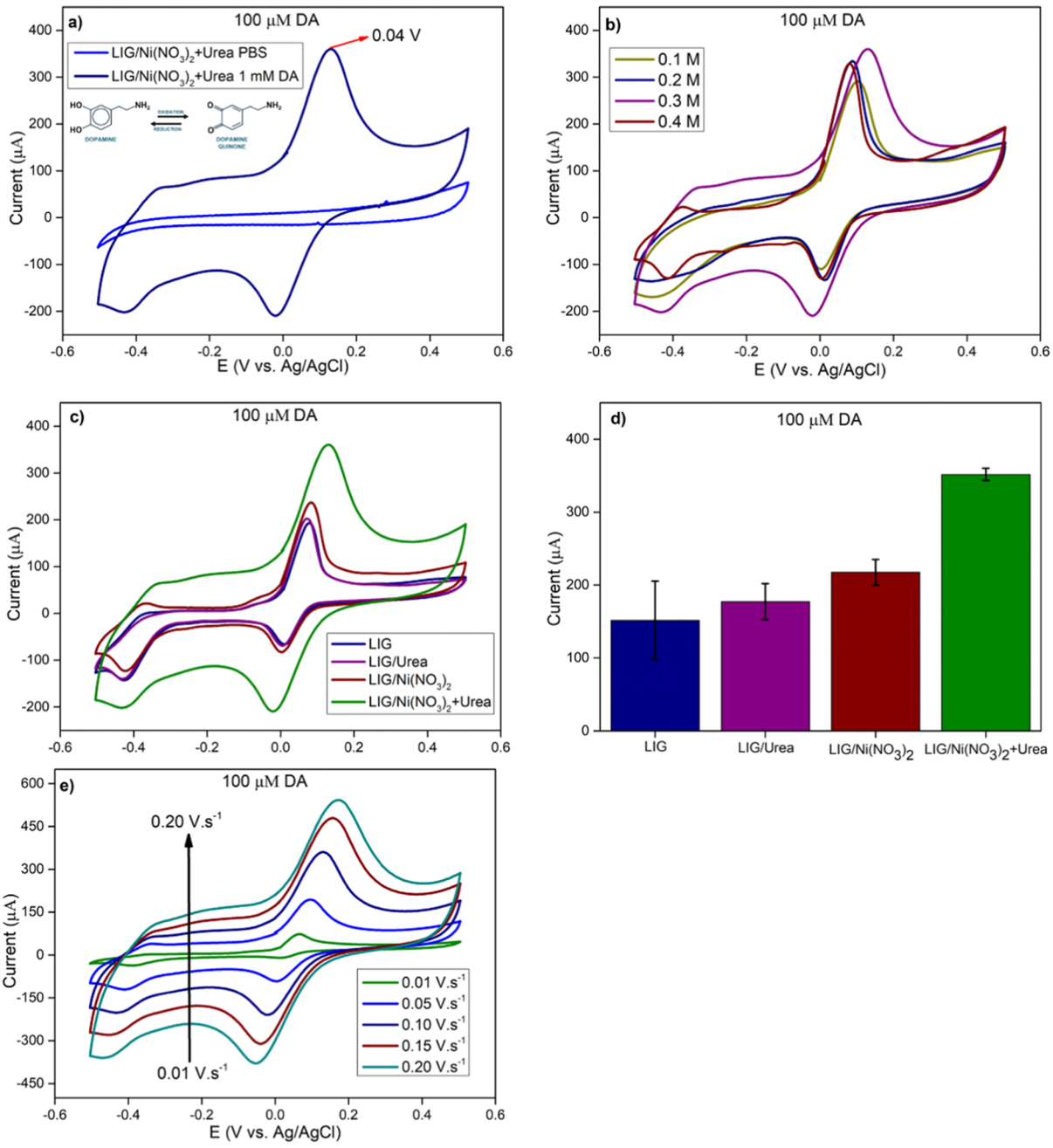

Figure 4. (a) CV of the LIG/$Ni(NO_3)_2$+ Urea sensor in PBS and 100 μmol·L^{-1} DA. Schematic representation of dopamine reversible redox to dopamine-quinone under electrochemical conditions, pH = 7.5. (b) Evaluation and performance of different urea concentrations 0.1 to 0.4 mol·L^{-1}in the sensor dispersion to optimize electrical current response. (c) CV comparative of the LIG sensor, LIG/Urea, LIG/$Ni(NO_3)_2$, and LIG/$Ni(NO_3)_2$ + Urea in the presence of 100 μmol·L^{-1}DA. (d) Performance of LIG, LIG/Urea, LIG/$Ni(NO_3)_2$, and LIG/$Ni(NO_3)_2$ + Urea sensors for the detection of 100 μmol·L^{-1} DA. (e) CV performed at different scan rates using the LIG/$Ni(NO_3)_2$+ Urea sensor for 100 μmol·L^{-1}DA in PBS at pH = 7.5, following the equation $I_p = (2.69 \times 10^5)\, n^{3/2} A D^{1/2} C^0 v^{1/2}$.

the dispersed nickel-based particles can act as selective redox centers for DA, promoting interactions with the nitrogen-containing groups.[30,44,50] The incorporation of nitrogen into the electrochemical sensor modulates its electronic properties by introducing active sites, which improve conductivity and electrocatalytic activity toward dopamine oxidation, resulting in enhanced sensitivity and selectivity.[51,52] Moreover, urea's biocompatibility supports its application in biological fluids such as blood, urine, and tears, expanding the sensor's potential for use in noninvasive systems.[53]

To further confirm the best-performing sample, LIG-based electrodes functionalized in different ways were tested using CV, with 100 μmol·L^{-1} DA as the analyte and PBS as the supporting electrolyte. CV curves in the absence and presence of 100 μmol·L^{-1} DA for LIG, LIG/Urea, and LIG/$Ni(NO_3)_2$ are shown in Figures S2, S3, and S4, respectively. Figure 4c shows the comparison of CV curves for unmodified LIG, LIG/Urea, LIG/$Ni(NO_3)_2$, and LIG/$Ni(NO_3)_2$ + Urea.

The redox processes involving nickel in alkaline environments can lead to interconversion between different nickel oxidation states, primarily Ni(II) and Ni(III). These processes

https://doi.org/10.1021/acsomega.6c03287
ACS Omega 2026, 11, 36141−36150

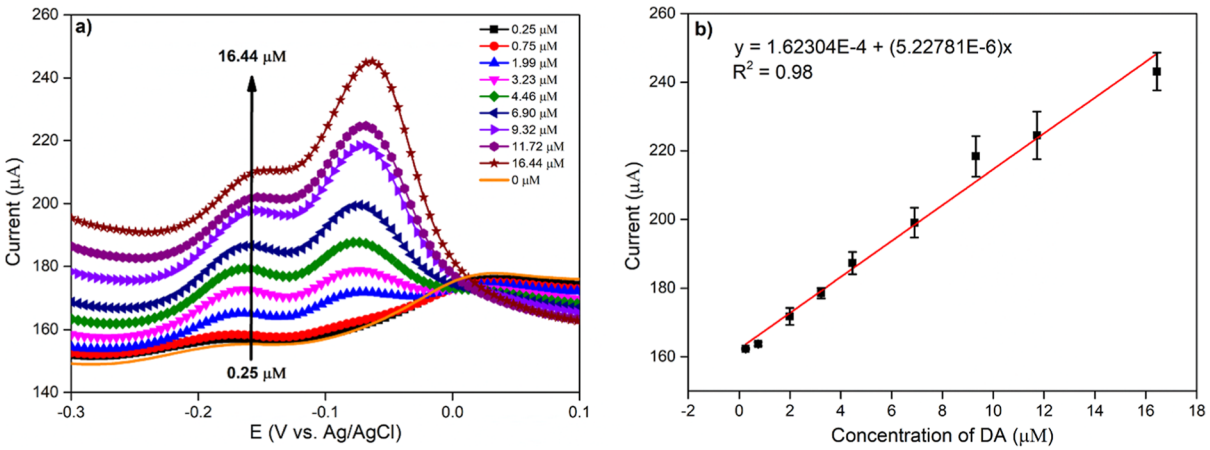

Figure 5. (a) DPV employed to evaluate the sensor's analytical performance for DA detection inserted in PBS solution. (b) Analytical curve of the sensor in PBS solution.

typically involve the formation of nickel hydroxides and oxyhydroxides on the electrode surface. The appearance of a shoulder at 0.2 V in the voltammetry of the LIG/Ni$(NO_3)_2$ sensor suggests an electrochemical process occurring at a very close potential. This feature could be attributed to a Ni(II)/Ni(III) redox transition at a specific nickel site or phase, which occurs at a potential slightly different from that of the main peak.[54] An alternative hypothesis is that a shoulder may appear if charge transfer is limited or if the process is diffusion-controlled within a certain potential range (the DA oxidation process), while another process with different kinetics (the Ni(II)/Ni(III) redox transition) occurs in parallel. The morphology of the electrode surface and the way nickel is deposited or incorporated can create different electrochemical environments, leading to variations in peak potentials.[55−57]

The LIG/Ni$(NO_3)_2$ + Urea sensor exhibits more pronounced and sharper redox peaks in the presence of DA, indicating significantly improved electrochemical performance. Thus, a significantly higher oxidation current was observed, as shown in Figure 4d. This increase can be attributed to the electrocatalytic properties of the modifiers, which facilitate electron transfer and amplify the sensor's signal, increasing its maximum current response and thereby expanding the detectable concentration range of DA.[58] The incorporation of nickel species plays a key role in facilitating redox mediation and improving the system's electron transfer kinetics. Additionally, the nitrogen functionalities introduced through urea doping enhance electrical conductivity and create additional active sites for DA adsorption. These synergistic effects result in reduced overpotential and increased peak current, leading to improved sensitivity and selectivity for DA detection.[59]

Figure 4e shows the behavior of the DA sensor at varying scan rates (from 0.01 V·s^{-1} to 0.20 V·s^{-1}), where the peak current increases linearly with the square root of the scan rate, which is characteristic of a diffusion-controlled process.[53−55] This indicates that the oxidation kinetics of DA on the sensor are governed by the diffusion of the analyte to the electrode surface. Furthermore, the electrochemical reaction is fast and reversible. Increasing the current range at higher scan rates enhances the sensor's dynamic sensitivity, enabling the detection of DA at lower concentrations by more efficiently renewing the diffusion layer.[56] The oxidation and reduction peak potentials are seen to be shifted toward more positive and negative areas, respectively, as the scan rate increases. This is consistent with a slower electron transfer mechanism at higher scan rates.[57]

To quantitatively substantiate the enhanced catalytic activity of the modified sensors, the electrochemical active surface area (ECSA) for all electrode compositions was determined by using the Randles−Sevcik equation. The calculated ECSA values were 3.27 cm^2 for pristine LIG, 3.44 cm^2 for LIG/Urea, 4.02 cm^2 for LIG/Ni$(NO_3)_2$, and a remarkable 13.36 cm^2 for the LIG/Ni$(NO_3)_2$ + Urea composite. The isolated addition of urea or nickel species resulted in only modest increases in the electroactive area. In stark contrast, the synergistic comodification promoted an approximately 4-fold enhancement in ECSA compared to the pristine material. This quantitative finding strongly corroborates the morphological evidence (Figure 2), demonstrating that the simultaneous thermal decomposition of urea and incorporation of nickel during laser induction creates a highly exfoliated, 3D porous network that maximizes the exposed active sites, thereby facilitating superior dopamine electrooxidation kinetics.

Tests were carried out to evaluate the performance of the LIG/Ni$(NO_3)_2$ + Urea sensors in terms of repeatability, reproducibility, and stability for the detection of dopamine in tear samples. The repeatability test (Figure S5) was performed with five successive measurements (n = 5). The relative standard deviation (RSD) was calculated, resulting in an RSD of 1.29%, which indicates that the LIG/Ni$(NO_3)_2$ + Urea electrochemical sensors exhibit a high repeatability. Reproducibility tests (Figure S6) were conducted using three different sensors in triplicate, yielding an RSD of 3.17%, confirming that the fabrication process is highly reproducible. The stability of the disposable sensor (Figure S7) was monitored over a 30-day period (1, 7, and 30 days). The results demonstrated that the sensor remains fully operational for point-of-care testing, maintaining an ideal performance for up to 7 days, with a gradual decrease in response observed by day 30.

Figure 5a displays the results of DPV for the LIG/Ni$(NO_3)_2$ + Urea sensor at various DA from 0.25 to 16.44 μmol·L^{-1}. DPV was selected due to its enhanced sensitivity compared to CV, as it minimizes capacitive current interference. Initial measurements were performed in PBS at pH 7.5 to establish a baseline, followed by incremental additions of DA. As the DA concentration increased, the oxidation current rose correspondingly. As depicted in Figure 5b, the current response showed a linear correlation (R^2 = 0,98) with DA concentration

https://doi.org/10.1021/acsomega.6c03287
ACS Omega 2026, 11, 36141−36150

Table 1. Comparison of Performance of Sensors from Other Authors with This Work

electrode	analyte	techniques	linear range (DA)	LOD (DA)	refs
rGO/ReO_3 nanocomposite-modified GCE	DA/UA/AA	DPV	10−152 nM	0.08 nM	61
$Nb_4C_3T_x$ MXene-AgNPs LIG	DA	CA	1.1−10 μM	1.0 nM	62
MoS_2/Au	DA	DPV	0.5−300 μM	76 nM	63
MoS_2-RGO	DA/UA/AD	DPV	MoS_2-RGO: 1−110 μM	MoS_2-RGO: 0.5 μM	64
BC_5N			BC_5N: 2.3−20 μM	BC_5N:2.1 μM	
rGO-SS	DA	DPV	1−1000 μM	1 μM	65
LIG/$Ni(NO_3)_2$ + urea	DA	DPV	0.25−16.44 μM	17.86 nM	This Work

within the tested range. Using the calibration curve, the limit of detection (LOD) and limit of quantification (LOQ) are calculated according to eqs 1 and 2,[60] where S is the standard deviation of the PBS samples.

$$\mathrm{LOD} = \frac{(3.3^{*}S)}{|\mathrm{Slope}|} \quad (1)$$

$$\mathrm{LOQ} = \frac{(10^{*}S)}{|\mathrm{Slope}|} \quad (2)$$

Based on the calibration data, the LOD and LOQ were 17.86 nmol·L^{-1} and 54.14 nmol·L^{-1}, respectively. The DPV results shown in Figure 5b revealed a highly linear response (R^2 = 0.98) across the tested dopamine concentration range. These performance metrics highlight the sensor's remarkable sensitivity and are consistent with those of other sensors reported in the literature, as shown in the comparative Table 1.

4. REAL SAMPLE ANALYSIS

Electrochemical detection of DA in biological fluids, such as tear fluid, represents a promising approach for noninvasive monitoring of neurological and metabolic disorders. Recovery experiments were performed by spiking the samples with the DA at four different concentration levels (3.23−9.32 μmol·L^{-1}). All measurements were carried out in triplicate (n = 3), and concentrations were calculated using the external standard method. The recovery values ranged from 99.7% to 100.1% (Table 2), with low RSD values, indicating the high accuracy and precision of the proposed sensor for DA determination in real matrices.

The electrochemical performance in synthetic tear fluid was evaluated within a concentration range relevant to clinical monitoring (3.23−9.32 μmol·L^{-1}). In this low-concentration regime, the sensor maintained a stable and linear increase in oxidation current (R^2 = 0.96), demonstrating that matrix-induced fouling is negligible under these conditions. However, it is important to note that the fouling phenomenon, characterized by the formation of an insulating polydopamine film, is a concentration-dependent process typically observed at much higher DA levels.[66−68] At the lower concentrations tested in this study, the porous LIG/$Ni(NO_3)_2$ + Urea architecture effectively mitigates surface passivation, ensuring that the analytical signal remains proportional to the analyte concentration. This confirms the sensor's reliability for dopamine detection in real-world tear samples without the interference of significant electrode fouling.

Furthermore, the error bars showed variations between 2% and 6%, indicating the precision and reliability of the proposed sensor. However, as shown in Figure S8, small variations in current during DA detection were observed, attributed to the presence of interferents in the synthetic tear fluid. Each interfering was analyzed individually to assess its impact on sensor performance.

Table 2. Application of LIG/$Ni(NO_3)_2$ + Urea Sensor for Determination DA in Synthetic Tear

sample	added DA (mol·L^{-1})	found DA (mol·L^{-1})[a]	recovery (sensor, %)[b]
synthetic tear	(3.23×10^{-6})	$(3.23 \pm 0.0103) \times 10^{-6}$	100
	(4.46×10^{-6})	$(4.46 \pm 0.0100) \times 10^{-6}$	100
	(6.90×10^{-6})	$(6.88 \pm 0.0085) \times 10^{-6}$	99.7
	(9.32×10^{-6})	$(9.33 \pm 0.0087) \times 10^{-6}$	100.1

[a] Average of 3 measured concentrations. [b] Recovery percentage = $\left(\frac{(\mathrm{Found})}{\mathrm{Added}}\right)\cdot 100$

5. CONCLUSION

This study reported the development of electrochemical sensors based on LIG for the detection of dopamine in both controlled environments and synthetic tear fluid. Optimization studies revealed that the functionalization of the working electrodes with 0.1 mol·L^{-1} $Ni(NO_3)_2$ and 0.3 mol·L^{-1} urea resulted in an improved performance for nonenzymatic electrochemical sensing of DA. Surface morphology analysis revealed significant differences between treated and untreated electrode, resulting in increased electroactive surface area and enhanced sensor performance. The sensor exhibited well-defined detection limits and a clear dynamic range for dopamine quantification. Notably, the incorporation of urea into the LIG/$Ni(NO_3)_2$ system increased the oxidation current in the presence of dopamine while maintaining high sensitivity, thereby improving selectivity and detection performance. In PBS solution, the sensor had a response in the detection range of 0.25−16.44 μmol·L^{-1} LOD of 17.86 nmol·L^{-1} and LOQ of 54.14 nmol·L^{-1}, with R^2 = 0.98. In synthetic tear fluid, the sensor maintained a reliable response with a linear range of 3.23−9.32 μmol·L^{-1}, with recovery for DA close to 100%. Notably, the direct laser fabrication of nickel-based microstructures represents a novel, cost-effective, and efficient strategy. The LIG/$Ni(NO_3)_2$ + Urea sensor demonstrated strong potential for nonenzymatic DA detection in both standard and biologically relevant samples, and the innovative laser synthesis method introduced here offers a promising path forward in electrochemical sensing.

■ ASSOCIATED CONTENT

Supporting Information

The Supporting Information is available free of charge at https://pubs.acs.org/doi/10.1021/acsomega.6c03287.

https://doi.org/10.1021/acsomega.6c03287
ACS Omega 2026, 11, 36141−36150

CHN elemental analysis data for nitrogen quantification across the different sensor configurations; FTIR spectrum of the LIG/Ni$(NO_3)_2$ sensor; cyclic voltammetry characterization of the pristine LIG, LIG/Urea, and LIG/Ni$(NO_3)_2$ sensors in the presence of dopamine; repeatability, reproducibility, and storage stability evaluations of the LIG/Ni$(NO_3)_2$ + Urea sensor configuration; and selectivity testing against potential interfering components in synthetic tears This material is available free of charge via the Internet at https://pubs.acs.org/journal/acsodf (PDF)

AUTHOR INFORMATION

Corresponding Author

Neftali Lenin Villarreal Carreno − *Graduate Program in Materials Science and Engineering, Technology Development Center, Federal University of Pelotas, 96010-000 Pelotas, Rio Grande do Sul, Brazil; Center for Embedded Devices and Research in Digital Agriculture (CEDRA), São Leopoldo, RS 93025-753, Brazil;* orcid.org/0000-0002-5780-817X; Email: neftali@ufpel.edu.br

Authors

Lucas Minghini Gonçalves − *Graduate Program in Materials Science and Engineering, Technology Development Center, Federal University of Pelotas, 96010-000 Pelotas, Rio Grande do Sul, Brazil; Center for Embedded Devices and Research in Digital Agriculture (CEDRA), São Leopoldo, RS 93025-753, Brazil*

Bruno Vasconcellos Lopes − *Graduate Program in Materials Science and Engineering, Technology Development Center, Federal University of Pelotas, 96010-000 Pelotas, Rio Grande do Sul, Brazil; Center for Embedded Devices and Research in Digital Agriculture (CEDRA), São Leopoldo, RS 93025-753, Brazil*

Bruno da Silveira Noremberg − *Graduate Program in Materials Science and Engineering, Technology Development Center, Federal University of Pelotas, 96010-000 Pelotas, Rio Grande do Sul, Brazil*

Raphael Dorneles Caldeira Balboni − *Graduate Program in Materials Science and Engineering, Technology Development Center, Federal University of Pelotas, 96010-000 Pelotas, Rio Grande do Sul, Brazil*

Guilherme Kurz Maron − *Graduate Program in Materials Science and Engineering, Technology Development Center, Federal University of Pelotas, 96010-000 Pelotas, Rio Grande do Sul, Brazil; Northern Regional Technological Institute (ITR Norte), Technological University of Uruguay (UTEC), 40000 Rivera/Rivera, Uruguay;* orcid.org/0000-0003-4918-0383

Anderson Thesing − *Institute of Physics, Universidade Federal do Rio Grande do Sul, Porto Alegre RS 91501-970, Brazil;* orcid.org/0000-0002-3655-9936

Daiane Dias − *Universidade Federal do Rio Grande (FURG) − School of Chemistry and Food, Rio Grande, RS 96203-900, Brazil*

Irene Teresinha Santos Garcia − *Federal University of Rio Grande do Sul, Department of Physical Chemistry, Porto Alegre, RS 91501-970, Brazil;* orcid.org/0000-0003-1647-5054

Sabir Khan − *Graduate Program in Materials Science and Engineering, Technology Development Center, Federal University of Pelotas, 96010-000 Pelotas, Rio Grande do Sul, Brazil;* orcid.org/0000-0003-4557-238X

Complete contact information is available at: https://pubs.acs.org/10.1021/acsomega.6c03287

Author Contributions

L.G.: formal analysis, investigation, methodology, visualization, and writing—original draft. B.L.: methodology, validation, investigation, supervision, and formal analysis. B.N.: formal analysis and writing—review and editing. R.B.: investigation, formal analysis, and writing—review and editing. G.M.: writing—review and editing. A.T.: formal analysis. D.D.: writing—review and editing. I.G.: formal analysis and writing—review and editing. S.K.: writing—review and editing. N.C.: conceptualization, supervision, resources, and project administration.

Funding

The Article Processing Charge for the publication of this research was funded by the Coordenacao de Aperfeicoamento de Pessoal de Nivel Superior (CAPES), Brazil (ROR identifier: 00x0ma614).

Notes

The authors declare no competing financial interest.

ACKNOWLEDGMENTS

The authors would like to thank the Coordenação de Aperfeiçoamento de Pessoal de Nível Superior (CAPES) − Finance cod 001, Fundação de Amparo à Pesquisa do Estado do Rio Grande do Sul (FAPERGS) (Grant no. 23.2551-0001907-8), (EDITAL FAPERGS 07/2021 − PROGRAMA PESQUISADOR GAÚCHO − PqG 21/2551-0002237-0), and Conselho Nacional de Desenvolvimento Científico e Tecnológico (CNPq) (Grant nos. 408075/2022-8 and 408869/2022-4). This work has been partially funded by the project AgroHealth, supported by the Center for Embedded Devices and Research in Digital Agriculture (CEDRA), with financial resources from the PPI IoT/Manufatura 4.0/PPI HardwareBR of the MCTI grant no. 056/2023, signed with EMBRAPII. The TOC graphic was created with the support of BioRender.com.

REFERENCES

(1) Wang, A. R.; Groome, A.; Taniguchi, L.; Eshel, N.; Bentzley, B. S. The Role of Dopamine in Reward-Related Behavior: Shining New Light on an Old Debate. *J. Neurophysiol.* **2020**, *124*, 309−311.

(2) Costanza, A.; Amerio, A.; Aguglia, A.; Escelsior, A.; Serafini, G.; Berardelli, I.; Pompili, M.; Amore, M. When Sick Brain and Hopelessness Meet: Some Aspects of Suicidality in the Neurological Patient. *CNS Neurol. Disord. Drug Targets* **2020**, *19* (4), 257−263.

(3) Keshavananda Prabhu, C. P.; Nemakal, M.; Aralekallu, S.; Mohammed, I.; Palanna, M.; Sajjan, V. A.; Akshitha, D.; Sannegowda, L. K. A Comparative Study of Carboxylic Acid and Benzimidazole Phthalocyanines and Their Surface Modification for Dopamine Sensing. *J. Electroanal. Chem.* **2019**, *847*, 113262.

(4) Sonia, J.; Kumara, B. N.; Pinto, K. J.; Hashim, A.; Priya, E. S. S.; Kalpana, B.; Thomas, R.; Sudhakara Prasad, K. Disposable Paper Electrodes for Detection of Changes in Dopamine Concentrations in Rat Brain Homogenates. *Talanta* **2024**, *274*, 125940.

(5) Woolf, P. D.; Akowuah, E. S.; Lee, L.; Kelly, M.; Feibel, J. Evaluation of the Dopamine Response to Stress in Man. *J. Clin. Endocrinol. Metabolism* **1983**, *56*, 246−250.

(6) Sharma, N. S.; Acharya, S. K.; Nair, A. P.; Matalia, J.; Shetty, R.; Ghosh, A.; Sethu, S. Dopamine Levels in Human Tear Fluid. *Indian J. Ophthalmol.* **2019**, *67* (1), 38−41.
(7) Ozdalgic, B.; Gul, M.; Uygun, Z. O.; Atçeken, N.; Tasoglu, S. Emerging Applications of Electrochemical Impedance Spectroscopy in Tear Film Analysis. *Biosensors* **2022**, *12*, 827.
(8) Goud, K. Y.; Moonla, C.; Mishra, R. K.; Yu, C.; Narayan, R.; Litvan, I.; Wang, J. Wearable Electrochemical Microneedle Sensor for Continuous Monitoring of Levodopa: Toward Parkinson Management. *ACS Sens.* **2019**, *4* (8), 2196−2204.
(9) Wang, Y. R.; Chuang, H. C.; Tripathi, A.; Wang, Y. L.; Ko, M. L.; Chuang, C. C.; Chen, J. C. High-Sensitivity and Trace-Amount Specimen Electrochemical Sensors for Exploring the Levels of β-Amyloid in Human Blood and Tears. *Anal. Chem.* **2021**, *93* (22), 8099−8106.
(10) Vilian, A. T. E.; An, S.; Choe, S. R.; Kwak, C. H.; Huh, Y. S.; Lee, J.; Han, Y. K. Fabrication of 3D Honeycomb-like Porous Polyurethane-Functionalized Reduced Graphene Oxide for Detection of Dopamine. *Biosens. Bioelectron.* **2016**, *86*, 122−128.
(11) C P, K. P.; Aralekallu, S.; Koodlur Sannegowda, L. Efficacy of Phthalocyanine-Based Catalysts in Electrochemical Sensors: A Comprehensive Review. *Adv. Sens. Res.* **2024**, *3* (12), 2400088.
(12) Li, Y.; Gu, Y.; Zheng, B.; Luo, L.; Li, C.; Yan, X.; Zhang, T.; Lu, N.; Zhang, Z. A Novel Electrochemical Biomimetic Sensor Based on Poly(Cu-AMT) with Reduced Graphene Oxide for Ultrasensitive Detection of Dopamine. *Talanta* **2017**, *162*, 80−89.
(13) Shantharaja; Nemakal, M.; Giddaerappa, G.; Gopal Hegde, S.; Koodlur Sannegowda, L. Novel Biocompatible Amide Phthalocyanine for Simultaneous Electrochemical Detection of Adenine and Guanine. *Microchem. J.* **2022**, *175*, 107223.
(14) Anuar, N. S.; Basirun, W. J.; Shalauddin, M.; Akhter, S. A Dopamine Electrochemical Sensor Based on a Platinum-Silver Graphene Nanocomposite Modified Electrode. *RSC Adv.* **2020**, *10* (29), 17336−17344.
(15) Wang, Z.; Cong, Y.; Fu, J. Stretchable and Tough Conductive Hydrogels for Flexible Pressure and Strain Sensors. *J. Mater. Chem.* **2020**, *8*, 3437−3459.
(16) Wang, J. Electrochemical Biosensors: Towards Point-of-Care Cancer Diagnostics. *Biosens. Bioelectron.* **2006**, *21*, 1887−1892.
(17) Kuntoji, G.; Kousar, N.; Gaddimath, S.; Koodlur Sannegowda, L. Macromolecule−Nanoparticle-Based Hybrid Materials for Biosensor Applications. *Biosensors* **2024**, *14*, 277.
(18) Anzar, N.; Hasan, R.; Tyagi, M.; Yadav, N.; Narang, J. Carbon Nanotube - A Review on Synthesis, Properties and Plethora of Applications in the Field of Biomedical Science. *Sens. Int.* **2020**, *1*, 100003.
(19) Lin, J.; Peng, Z.; Liu, Y.; Ruiz-Zepeda, F.; Ye, R.; Samuel, E. L. G.; Yacaman, M. J.; Yakobson, B. I.; Tour, J. M. Laser-Induced Porous Graphene Films from Commercial Polymers. *Nat. Commun.* **2014**, *5*, 5714.
(20) Xing, X.; Zou, Y.; Zhong, M.; Li, S.; Fan, H.; Lei, X.; Yin, J.; Shen, J.; Liu, X.; Xu, M.; Jiang, Y.; Tang, T.; Qian, Y.; Zhou, C. A Flexible Wearable Sensor Based on Laser-Induced Graphene for High-Precision Fine Motion Capture for Pilots. *Sensors* **2024**, *24* (4), 1349.
(21) Lopes, B. V.; Maron, G. K.; Masteghin, M. G.; Balboni, R. D. C.; Silva, S. R. P.; Carreno, N. L. V. Direct-Detection of Glyphosate in Drinking Water via a Scalable and Low-Cost Laser-Induced Graphene Sensor. *Anal. Methods* **2025**, *17*, 808.
(22) Fernandes Loguercio, L.; Thesing, A.; da Silveira Noremberg, B.; Vasconcellos Lopes, B.; Kurz Maron, G.; Machado, G.; Pope, M. A.; Lenin Villarreal Carreno, N. Direct Laser Writing of Poly (Furfuryl Alcohol)/Graphene Oxide Electrodes for Electrochemical Determination of Ascorbic Acid. *ChemElectroChem* **2022**, *9* (17), No. e202200334.
(23) Zhang, H.; Yan, Q.; Peng, Y.; Cai, Z.; Wan, C. Upgrading Lignin into Graphene-Based Materials: State of the Art and Perspectives. *Adv. Energy Sustain. Res.* **2024**, *5*, 2300252.
(24) Meng, L.; Chirtes, S.; Liu, X.; Eriksson, M.; Mak, W. C. A Green Route for Lignin-Derived Graphene Electrodes: A Disposable Platform for Electrochemical Biosensors. *Biosens. Bioelectron.* **2022**, *218*, 114742.
(25) Hall, D. S.; Lockwood, D. J.; Bock, C.; MacDougall, B. R. Nickel Hydroxides and Related Materials: A Review of Their Structures, Synthesis and Properties. *Proc. R. Soc. A* **2015**, *471*, 20140792.
(26) Yildirim, Y. E.; Güler, M. Development of a Functionalized SiO2 Supported Ni Nanoparticles Based Non-Enzymatic Amperometric Dopamine Sensor. *Bitlis Eren Üniversitesi Fen Bilimleri Dergisi* **2024**, *13* (4), 999−1012.
(27) Reid, R. C.; Minteer, S. D.; Gale, B. K. Contact Lens Biofuel Cell Tested in a Synthetic Tear Solution. *Biosens. Bioelectron.* **2015**, *68*, 142−148.
(28) Abdulhafez, M.; Tomaraei, G. N.; Bedewy, M. Fluence-Dependent Morphological Transitions in Laser-Induced Graphene Electrodes on Polyimide Substrates for Flexible Devices. *ACS Appl. Nano Mater.* **2021**, *4* (3), 2973−2986.
(29) Shokurov, A. V.; Menon, C. Laser-Induced Graphene Electrodes for Electrochemistry Education and Research. *J. Chem. Educ.* **2023**, *100* (6), 2411−2417.
(30) Wang, F.; Dong, X.; Wang, K.; Duan, W.; Gao, M.; Zhai, Z.; Zhu, C.; Wang, W. Laser-Induced Nitrogen-Doped Hierarchically Porous Graphene for Advanced Electrochemical Energy Storage. *Carbon N. Y.* **2019**, *150*, 396−407.
(31) Cheng, L.; Yeung, C. S.; Huang, L.; Ye, G.; Yan, J.; Li, W.; Yiu, C.; Chen, F. R.; Shen, H.; Tang, B. Z.; Ren, Y.; Yu, X.; Ye, R. Flash Healing of Laser-Induced Graphene. *Nat. Commun.* **2024**, *15* (1), 2925.
(32) Zhou, F.; Gai, L.; Liu, H.; Qin, D.; Abudouwufu, T.; Liu, Y. Enhanced Electrochemical Detection of Dopamine and Uric Acid Using Au@Ni-MOF and Employing 2D Structure DFT Simulation. *Sci. Rep.* **2025**, *15* (1), 8686.
(33) Paisanpisuttisin, A.; Poonwattanapong, P.; Rakthabut, P.; Ariyasantichai, P.; Prasittichai, C.; Siriwatcharapiboon, W. Sensitive Electrochemical Sensor Based on Nickel/PDDA/Reduced Graphene Oxide Modified Screen-Printed Carbon Electrode for Nitrite Detection. *RSC Adv.* **2022**, *12* (45), 29491−29502.
(34) Cui, M.; Xin, P.; Che, Z.; Zou, M.; Zhang, M.; Sun, X.; Yuan, Y.; Zou, Z.; Lv, G.; Wang, S.; et al. Highly Anti-Interference Electrocatalytic Sensing for Dopamine with Nitrogen-Doped Graphdiyne Directly in Biofluids. *Chem. Eng. J.* **2023**, *464*, 142629.
(35) Lee, Y.; Low, M. J.; Yang, D.; Nam, H. K.; Le, T. S. D.; Lee, S. E.; Han, H.; Kim, S.; Vu, Q. H.; Yoo, H.; Yoon, H.; Lee, J.; Sandeep, S.; Lee, K.; Kim, S. W.; Kim, Y. J. Ultra-Thin Light-Weight Laser-Induced-Graphene (LIG) Diffractive Optics. *Light: Sci. Appl.* **2023**, *12*, 146.
(36) Chen, C.; Yang, C. *Laser-Induced Nitrogen-Doped Graphene for High-Performance Flexible Supercapacitors*, 2020.
(37) Velasco, A.; Ryu, Y. K.; Hamada, A.; de Andrés, A.; Calle, F.; Martinez, J. Laser-Induced Graphene Microsupercapacitors: Structure, Quality, and Performance. *Nanomaterials* **2023**, *13* (5), 788.
(38) Varma, R.; Vasudevan, S. Extraction, Characterization, and Antimicrobial Activity of Chitosan from Horse Mussel Modiolus Modiolus. *ACS Omega* **2020**, *5* (32), 20224−20230.
(39) Devassy, A. M. C.; Kamalakshan, A.; Jamuna, N. A.; Ansilda, R.; Mandal, S. Enhanced Catalytic Activity of a New Nanobiocatalytic System Formed by the Adsorption of Cytochrome c on Pluronic Triblock Copolymer Stabilized MoS2Nanosheets. *ACS Omega* **2022**, *7* (19), 16593−16604.
(40) Du, F.; Xian, X.; Tang, P.; Li, Y. Catalytic Degradation of Lignin over Sulfonyl-Chloride-Modified Lignin-Based Porous Carbon-Supported Metal Phthalocyanine: Effect of Catalyst Concentrations. *Molecules* **2024**, *29* (2), 347.
(41) Rudolph, W. W.; Fischer, D.; Irmer, G. Hydration and Ion-Pair Formation of NaNO3(Aq): A Vibrational Spectroscopic and Density Functional Theory Study. *Appl. Spectrosc.* **2021**, *75* (4), 395−411.

https://doi.org/10.1021/acsomega.6c03287
ACS Omega 2026, 11, 36141−36150

(42) Bazan-Aguilar, A.; García, G.; Pastor, E.; Rodríguez, J. L.; Baena-Moncada, A. M. In-Situ Spectroelectrochemical Study of Highly Active Ni-Based Foam Electrocatalysts for Hydrogen Evolution Reaction. *Appl. Catal., B* **2023**, *336*, 122930.
(43) Mangrio, S.; Tahira, A.; Chang, A. S.; Mahar, I. A.; Markhand, M.; Shah, A. A.; Medany, S. S.; Nafady, A.; Dawi, E. A.; Saleem, L. M. A.; Mustafa, E. M.; Vigolo, B.; Ibupoto, Z. H. Advanced Urea Precursors Driven NiCo2O4 Nanostructures Based Non-Enzymatic Urea Sensor for Milk and Urine Real Sample Applications. *Biosensors* **2023**, *13* (4), 444.
(44) Rangaswamy, R.; Manohara, S. R.; Supritha, K. M.; Arun Kumar, N. S. Fabrication of Nickel Aluminate Based Electrochemical Sensor for Dopamine Detection. *Hybrid Adv.* **2024**, *6*, 100221.
(45) Lv, G.; Yang, M.; Pan, Y.; Fan, Y.; Zuo, J.; Liu, X.; Chen, J.; Zhang, S. High-Sensitive Electrochemical Sensor Based on Ni/NiCx-Integrated Functional Carbon Nanotubes for Simultaneous Determination of Acetaminophen and Dopamine. *Colloids Surf. A Physicochem. Eng. Asp.* **2024**, *703*, 135428.
(46) Xiong, Q.; Wan, H.; Peng, X.; Zhu, Y. An Ultra-Sensitive Electrochemical Dopamine Sensor Based on Ni@N-Doped Carbon Derived from COF LZU-1 Microspheres. *Ionics* **2023**, *29* (9), 3795−3803.
(47) Arif, H.; Sajid, A.; Ali, A.; Ahmed, N.; Iqbal, M.; Akyürekli, S.; Kaleli, M.; Alwadai, N.; Shafique, U.; Nazir, A. Selective Non-Enzymatic Electrochemical Detection of Dopamine Using Nickel Molybdate Nano-Dots Anchored on CNT Fiber Microelectrodes. *RSC Adv.* **2025**, *15* (43), 36596−36606.
(48) Ahmed, Y. M.; Eldin, M. A.; Galal, A.; Atta, N. F. Electrochemical Sensor for Simultaneous Determination of Trifluoperazine and Dopamine in Human Serum Based on Graphene Oxide-Carbon Nanotubes/Iron-Nickel Nanoparticles. *RSC Adv.* **2023**, *13* (36), 25209−25217.
(49) Balkourani, G.; Brouzgou, A.; Tsiakaras, P. A Review on Recent Advancements in Electrochemical Detection of Dopamine Using Carbonaceous Nanomaterials. *Carbon* **2023**, *213*, 118281.
(50) Tammina, S. K.; Yang, D.; Koppala, S.; Cheng, C.; Yang, Y. Highly Photoluminescent N, P Doped Carbon Quantum Dots as a Fluorescent Sensor for the Detection of Dopamine and Temperature. *J. Photochem. Photobiol., B* **2019**, *194*, 61−70.
(51) Minta, D.; González, Z.; Wiench, P.; Gryglewicz, S.; Gryglewicz, G. N-Doped Reduced Graphene Oxide/Gold Nanoparticles Composite as an Improved Sensing Platform for Simultaneous Detection of Dopamine, Ascorbic Acid, and Uric Acid. *Sensors* **2020**, *20*, 4427.
(52) Wang, H.; Seemakurthi, R. R.; Chen, G. F.; Strauss, V.; Savateev, O.; Hai, G.; Ding, L.; López, N.; Wang, H.; Antonietti, M. Laser-Induced Nitrogen Fixation. *Nat. Commun.* **2023**, *14* (1), 5668.
(53) Nong, J.; Zhang, N.; Wen, A.; Hu, C. Anti-Biofouling Laser-Scribed Graphene Electrochemical Sensor for Reliable Detection of Uric Acid in Human Saliva. *J. Electroanal. Chem.* **2024**, *952*, 117982.
(54) Gutierrez, C.; Salvador; Yamaguti, P.; Sato, S. *J. Electrochem. Soc.*, **1989**, *136*.
(55) Lyons, M. E. G.; Doyle, R. L.; Godwin, I.; O'Brien, M.; Russell, L. Hydrous Nickel Oxide: Redox Switching and the Oxygen Evolution Reaction in Aqueous Alkaline Solution. *J. Electrochem. Soc.* **2012**, *159* (12), H932−H944.
(56) Raeisi-Kheirabadi, N.; Nezamzadeh-Ejhieh, A.; Aghaei, H. Cyclic and Linear Sweep Voltammetric Studies of a Modified Carbon Paste Electrode with Nickel Oxide Nanoparticles toward Tamoxifen: Effects of Surface Modification on Electrode Response Kinetics. *ACS Omega* **2022**, *7* (35), 31413−31423.
(57) Seghiouer, A.; Chevalet, J.; Barhoun, A.; Lantelme, F. Electrochemical Oxidation of Nickel in Alkaline Solutions: A Voltammetric Study and Modelling. *J. Electroanalytical Chem.* **1998**, *442*, 113−123.
(58) Wang, Y.; Wang, D.; Dong, S.; Qiao, J.; Zeng, Z.; Shao, S. A Visible-Light-Driven Photoelectrochemical Sensing Platform Based on the BiVO4/FeOOH Photoanode for Dopamine Detection. *Electrochim. Acta* **2022**, *414*, 140207.
(59) Ambrogi, E. K.; Mirica, K. A. Electronic Chemical Sensors Based on Conductive Framework Materials. *Anal. Chem.* **2025**, *97*, 4253.
(60) Dos Santos, P. M.; Gorla, F. A.; Wong, A.; Corazza, M. Z.; Sotomayor, M. D. P. T.; Tarley, C. R. T. Voltammetric Determination of Cadmium Using Magnetic Graphite-Epoxy Composite Electrode Modified with Magnetic Nanoparticles. *Talanta* **2025**, *292*, 127982.
(61) Manna, S.; Kumar, S.; Sharma, A.; Sahoo, S.; Dey, M. K.; Mishra, P. K.; Satpati, A. K. RGO/ReO3 Nano Composite Modified Electrode for the Ultra-Sensitive Determination of Dopamine and Uric Acid. *Biosens. Bioelectron.:X* **2022**, *11*, 100156.
(62) Shinde, M.; Ramulu Torati, S.; Slaughter, G. Nb4C3Tx MXene-AgNPs Decorated Laser-Induced Graphene for Selective Detection of Dopamine. *J. Electroanal. Chem.* **2024**, *959*, 118180.
(63) Chen, H.; Chen, H.; Hong, R. Fabrication of Au Nanoparticle-Decorated Mos2 Nanoslices as Efficient Electrocatalysts for Electrochemical Detection of Dopamine. *Catalysts* **2019**, *9* (8), 653.
(64) Pramoda, K.; Moses, K.; Maitra, U.; Rao, C. N. R. Superior Performance of a MoS2-RGO Composite and a Borocarbonitride in the Electrochemical Detection of Dopamine, Uric Acid and Adenine. *Electroanalysis* **2015**, *27* (8), 1892−1898.
(65) Farajikhah, S.; Innis, P. C.; Paull, B.; Wallace, G. G.; Harris, A. R. Facile Development of a Fiber-Based Electrode for Highly Selective and Sensitive Detection of Dopamine. *ACS Sens.* **2019**, *4*, 2599−2604.
(66) Delmo, N.; Mostafiz, B.; Ross, A. E.; Suni, J.; Peltola, E. Developing an Electrochemical Sensor for the in Vivo Measurements of Dopamine. *Sens. Diagnostics* **2023**, *1*, 559−581.
(67) Wang, M.; Zheng, J.; Zhang, G.; Lu, S.; Zhou, J. Wearable Electrochemical Glucose Sensors for Fluid Monitoring: Advances and Challenges in Non-Invasive and Minimally Invasive Technologies. *Biosensors* **2025**, *15*, 309.
(68) Szewczyk, J.; Aguilar-Ferrer, D.; Coy, E. Polydopamine Films: Electrochemical Growth and Sensing Applications. *Eur. Polym. J.* **2022**, *174*, 111346.

https://doi.org/10.1021/acsomega.6c03287
ACS Omega 2026, 11, 36141−36150